

Heat flow in the Sea of Marmara Central Basin: Possible implications for the tectonic evolution of the North Anatolian fault

Céline Grall^{1,3*}, Pierre Henry¹, Devrim Tezcan², Bernard Mercier de Lepinay⁴, Anne Bécel¹, Louis Géli³, Jean-Luc Rudkiewicz⁵, Tiphaine Zitter¹, and François Harmegnies³

¹Aix-Marseille University, CEREGE, CNRS, UMR 6635, 13545 Aix-en-Provence cedex 4, France

²Institute of Marine Sciences, Middle East Technical University, 33731 Erdemli-Mersin, Turkey

³IFREMER, Marine Geosciences, 29280 Plouzané, France

⁴GEOAZUR, 250 rue Albert Einstein, Sophia-Antipolis 06560 Valbonne, France

⁵IFP, 1-4, Av. de Bois-Préau 92852 Rueil-Malmaison Cedex, France

ABSTRACT

The Central Basin in the Sea of Marmara is a syntectonic basin related to the evolution of the North Anatolian fault. A well-dated (ca. 15.5–16 ka) homogenite sediment can be used as a marker in three-dimensional depth model calculations, allowing a precise determination of the seafloor subsidence rates during the Holocene. A steady-state model based on the propagation of the rates downward through the basin fill provides a good correlation with the deeper seismic reflection imagery for the past 250 ka but indicates variation of subsidence pattern for older ages. Heat flow measured at the seafloor is affected by sedimentation blanketing effects. Heat flow and subsidence data can only be reconciled if the Central Basin depocenter migrated northward with time. According to that scenario, subsidence and deposition started earlier (ca. 5–3.5 Ma) in the southern subbasin, and an acceleration of subsidence in the northern subbasin occurred at ca. 2.5–1.5 Ma. These results allow us to propose that a southern fault system distinct from the Main Marmara fault is responsible for the southern onset of the subsidence. Changes in the fault network and slip rates are implied during the last 2.5–1.5 Ma despite no apparent change since 250 ka.

INTRODUCTION

The North Anatolian fault (NAF, Fig. 1) is a case study of transform plate boundary initiation in continental lithosphere. The NAF is thought to have initiated 13–11 Ma ago at its eastern end in the Arabia-Eurasia collision zone, but 5 Ma ago at the earliest in the Sea of Marmara area near its western end (Şengör, 1985; Armijo et al., 1999). This fault propagation has been modeled as a mode II crack in an elastic medium (Hubert-Ferrari et al., 2003). Alternatively, the NAF may have formed by progressive strain localization within a broad deformation zone, whose initial width was laterally variable and controlled by rheological heterogeneities of the lithosphere (Şengör et al., 2005).

In western Turkey, the Sea of Marmara area appears as a large-scale releasing bend on the northern branch of the NAF (Fig. 1), and has been interpreted as a pull-apart system (Armijo et al., 2002). In one end-member scenario, a major reorganization of the fault network with the activation of the Main Marmara fault (MMF) occurred as recently as 200 ± 100 ka ago (Le Pichon et al., 2001; Rangin et al., 2004). On the other hand, other authors see no evidence of strain localization on a single fault (Parke et al., 1999, 2002).

The history of subsidence in the syntectonic basins is a key to constrain the evolution of the fault network with time, as subsidence rates computed from mechanical or kinematic models with assumed fault geometries may be compared with observed subsidence patterns (Seeber et al., 2006; Hergert and Heidbach, 2010; Muller and Aydin, 2005). Muller and Aydin (2005) concluded that the total subsidence since the Miocene

*E-mails: grall@cerege.fr; henry@cerege.fr; devrim@ims.metu.edu.tr; bmercier@geoazur.unice.fr; Bécel@u-3mrs.fr; Louis.Geli@ifremer.fr; J-Luc.RUDKIEWICZ@ifp.fr; zitter@cerege.fr; Francois.Harmegnies@ifremer.fr.

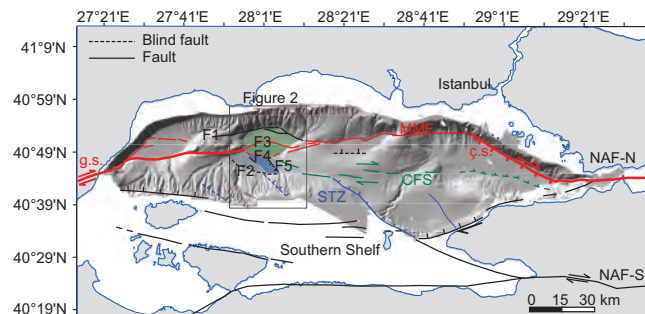


Figure 1. Tectonic sketch map of Sea of Marmara region. NAF-N and NAF-S are northern and southern segments of the North Anatolian fault (Seeber et al., 2006). Red is the Main Marmara fault (MMF; Le Pichon et al., 2001). Red thick lines are the two main segments of the MMF: the Ganos segment (g.s.) and the Çınarcık segment (ç.s.). Blue is the South Transensional Zone (STZ). Green is the Central fault system (CFS). The fault system on the Southern Shelf is from Parke et al. (1999). Rectangle locates Figure 2 and the Central Basin. Blue area is the southern subbasin of the Central Basin. Green area is the northern subbasin of the Central Basin. Detail mapping of the faults within the Central Basin is also proposed.

is better reproduced by the steady-state fault network proposed by Armijo et al. (2002) than by other models (Parke et al., 2002; Le Pichon et al., 2001). However, this work did not take into account observed changes in the location of the main depocenter in Çınarcık Basin (Carton et al., 2007). In the Central Basin, interpretation of seismic reflectors in terms of glacio-eustatic sequencing suggests a minimum age of 3 Ma for the onset of subsidence (Laigle et al., 2008). However, seismic surveys reveal that the basin structure is more complex than suggested by its symmetrical seafloor morphology (e.g., Bécel et al., 2010). We propose here to model the subsidence history of the Central Basin and discuss the implications for the evolution of the NAF system in the Sea of Marmara. A remarkable feature of this basin is the presence of dated homogenite (Beck et al., 2007), which can be used to determine Holocene subsidence rates. We test how far in the past these subsidence rates may be extrapolated by combining these with seismic reflection data and by comparing basin thermal modeling results with heat flow data.

HOLOCENE SUBSIDENCE RATE AND STEADY-STATE MODEL

A transparent layer in sediment sounding profiles acquired in the Central Basin (Figs. 2A and 2B) was cored and interpreted as a tsunami-related deposit of the homogenite type, in which long-lasting current oscillations caused an almost complete segregation between the coarse basal layer and suspended silt and clay particles (Beck et al., 2007). Plant debris dated with ¹⁴C gives a calibrated age of 15.5–16 kyr B.P. for this event (Beck et al., 2007). The thickness of this layer varies laterally, reaching ~12 m in the depocenter and pinching out toward the edges (Fig. 2A). From the deposition process, it is inferred that the top of the homogenite was horizontal when it settled. Consequently, the depth of the top of

$$V_0(1 - \phi_0) \cdot t = H - \frac{\phi_0}{a}(1 - e^{-aH}). \quad (1)$$

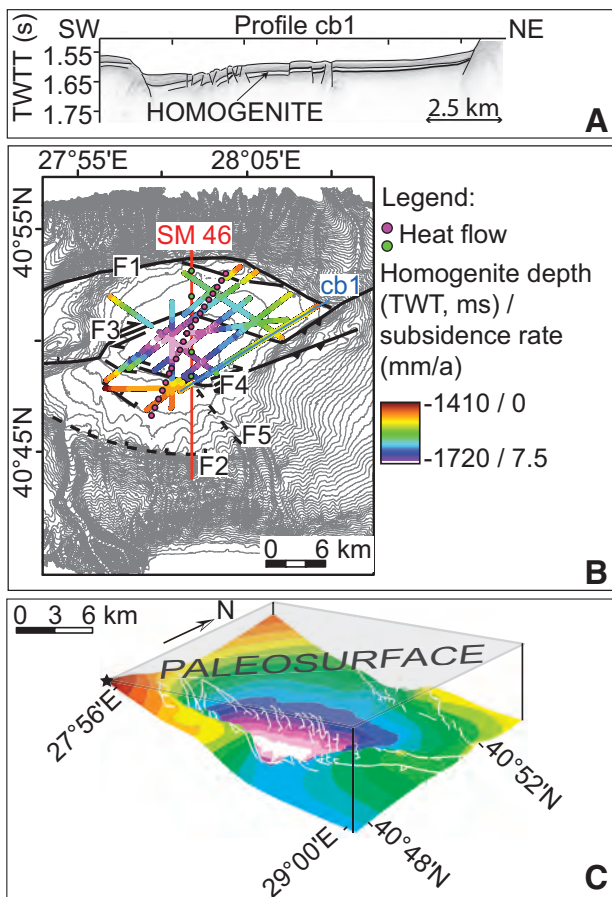


Figure 2. Three-dimensional model of subsidence rate according to the homogenite paleosurface reference. **A:** Chirp profile cb1. Arrow points to a homogenite layer (Beck et al., 2007). **B:** Two-way travel-time and subsidence rates computed along the chirp profiles. Pink and green dots are spring (2007) and autumn (2009) heat flow stations, respectively. Note locations of faults F1, F2, F3, F4, and F5 and seismic line SM46. **C:** Three-dimensional model of subsidence rate since deposition of the homogenite, obtained by interpolation. Color scale is the same as in Figure 2B. Black star marks location of the minimum homogenite depth.

the homogenite with respect to its pinching point is a measurement of relative seafloor subsidence, and may also be considered as the minimum absolute subsidence (Fig. 2C). The top of the Central Basin homogenite was picked on chirp profiles (MARMARASCARPS cruise, Fig. 2B) and interpolated using an iterative finite-difference algorithm available with ArcGIS (Fig. 2C) (Hutchinson and Dowling, 1991). The relative subsidence rate is calculated assuming a 15.5 ka age for the homogenite. We obtain a maximum subsidence rate of ~ 7.5 mm/a in the depocenter of the basin (Figs. 2B and 2C).

We use a steady-state compaction model to propagate the present subsidence rate downward through the basin fill (Hutchison, 1985). In this model the sedimentation rate is constant with time, and porosity variation with depth is given by Athy's law, $\phi(z) = \phi_0 \exp[-a(z - z_0)]$, where ϕ_0 is the porosity of the sediment on the seafloor, z_0 is seafloor depth, and a is Athy's constant. We used average parameters proposed for clay-rich turbidite series deposited in deep sea trenches: $\phi_0 = 0.7$ and $a = 0.67 \text{ km}^{-1}$ (Le Pichon et al., 1990). The solid particle flux V_s is related to the sedimentation rate V_0 at the seafloor by $V_s = V_0(1 - \phi_0)$ and, at any given time, is invariant over the sedimentary column. Assuming steady-state solid particle flux, the rate of burial, $V(z)$, decreases with depth according to $V(z) = V_0 C(1 - \phi_0) / (1 - \phi_0)$, and the theoretical depth H ($H = z - z_0$) for a horizon of age t is given by solving the equation (Hutchison, 1985)

The Holocene sedimentation observed in the Sea of Marmara deep basins is ~ 3 mm/a and was two or three times higher during glacial times (Çağatay et al., 2003). We assume that, averaged over time, sedimentation rate compensates for subsidence rate, and thus use the subsidence rates at the seafloor evaluated from the deformation of the 15.5 ka homogenite in place of V_0 . We apply equation 1 and calculate the theoretical depth of horizons at 130 ka, 250 ka, 330 ka, 450 ka, 1 Ma, 1.5 Ma, 2 Ma, and 5 Ma (model I, Fig. 3A). During the last glacial cycle, the Sea of Marmara was isolated at the beginning of Marine Isotope Stage (MIS) 4 and reconnected ca. 14,700 yr B.P., which is compatible with a sill depth of ~ 80 m in Çanakkale Strait (Çağatay et al., 2009). Considering global sea-level estimations (Siddall et al., 2003) and benthic foraminifer $\delta^{18}\text{O}$ records (Lisiecki and Raymo, 2005), lacustrine to marine transitions followed by rapid water level rise are expected in the Sea of Marmara at 130 ka, 250 ka, 335 ka, 430 ka, and 640 ka. We hypothesize that these events determine the boundaries of stratigraphic sequences, although we have no independent constraints on the age of the seismic reflectors.

The theoretical 130 ka and 250 ka horizons coincide with strong seismic reflectors, suggesting that the subsidence pattern did not change over the past 250 ka (compare the shape of the sequence boundaries between model I and model II in Fig. 3A). For older ages, computed horizons progressively deviate from seismic reflectors, as the model apparently underestimates past vertical motion along fault F3. Moreover, the model would result in the filling of the basin in 2 Ma in the center and in the north of the basin, but in 5 Ma in the south between F2 and F5 (Fig. 3A). Correlation of sedimentary reflectors across the poorly reflective zone between F4 and F5 is uncertain, leaving many possible solutions. In the following we use thermal modeling to assess whether the inferred subsidence rates are consistent with heat flow data.

HEAT FLOW DATA AND THERMAL MODELING IMPLEMENTATION

Heat flow measurements were carried out with 6-m-long gravity corers instrumented with six autonomous thermistor probes. Probes were intercalibrated before each penetration, and equilibrium temperatures in the sediment were determined by $1/t$ regression on an 8 min record that starts at probe penetration. Absolute temperature precision is ~ 0.01 K and relative measurements have a 1 mK accuracy. A transect of 20 temperature gradient measurements was done in spring 2007 (MARNAUT cruise), and four measurements were done in autumn 2009 along the SM46 (N-S) seismic line (MARMESONET cruise). Slightly lower gradients in the autumn data set can be explained by (presumably seasonal) variations of bottom water temperature of ~ 0.01 °C. Thermal conductivity measurements performed on cores with a needle probe displayed little variability near $0.84 \pm 0.07 \text{ W m}^{-1} \text{ K}^{-1}$, so heat flow is computed assuming constant conductivity. All errors result in an uncertainty of $\sim 10\%$ in the heat flow data. Heat flow data from onshore boreholes around the Sea of Marmara range from 35 to 115 mW/m^2 (Pfister et al., 1998). In the Thrace Basin area, the average heat flow is 57 mW/m^2 . South of the Sea of Marmara, heat flow is influenced by crustal extension and hydrothermalism, and appears higher and more scattered, with an average of 85 mW/m^2 .

The heat flow profile acquired during spring (2007) presents an asymmetric U shape (Fig. 3B). At the center of the basin, values reach a minimum lower than 20 mW/m^2 , and this very low heat flow in the Central Basin is presumably due to the sediment blanketing effect (Lucazeau and Le Douaran, 1985). Additionally, the thermal conductivity contrast between the sediments and the basement deflects heat flow away from the basin, resulting in spatial variations. We used the TEMIS (e.g., Rudkiewicz et al., 2000) basin modeling software to calculate heat flow at the seafloor in two dimensions. Fluid flow (Darcy) and heat equations are

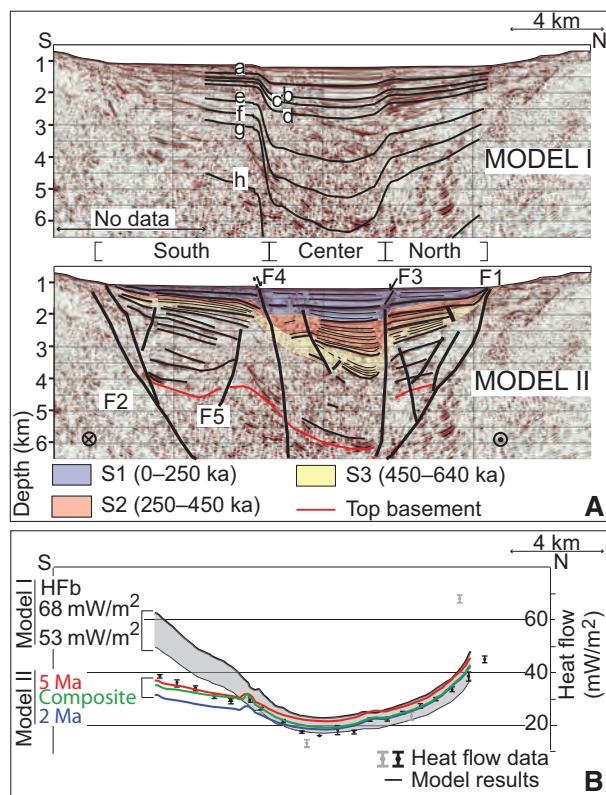


Figure 3. Basin models and thermal modeling responses. A: Basin models. Model I is a steady-state basin model along the SM46 seismic line (Bécel et al., 2010). Letters a, b, c, d, e, f, g, and h stand for 130 ka, 250 ka, 330 ka, 450 ka, 1 Ma, 1.5 Ma, 2 Ma, and 5 Ma, respectively. Model II is an interpreted seismic profile where three main sequences, the basement, and the faults are drawn. Note how the sequence boundaries for older strata differ from modeled boundaries of model I. B: Heat flow data and thermal modeling results. Gray and black dots are spring (2007) and autumn (2009) heat flow data, respectively. For the location of heat flow station, refer to Figure 2B. Area and lines correspond to thermal modeling results. Gray area bounded by black lines: model I results for different basal heat flow values (HFb) indicated at left. Model I here is a steady-state basin of 2 Ma along the heat flow profile collected during the spring (2007). Red, green, and blue lines: model II results for three different basement ages. Blue: modeling for 2 Ma basement. Red: modeling for 5 Ma basement. Green: modeling for the southern subbasin of 5 Ma and the northern subbasin of 2 Ma. The green model is the better-fit model proposed. The basal heat flow is adjusted to ~ 68 mW/m². For thermal modeling parameters and exact basin models, see the GSA Data Repository (see footnote 1).

solved in transient state with a cell-centered finite-volume method in space and an implicit Euler integration in time (Rudkiewicz et al., 2000). This model takes into account compaction and fluid movements. In the absence of boreholes, the physical properties of the basin sediments and underlying basement are assumed (Table DR1 in the GSA Data Repository¹). The thermal conductivity of the basement is calculated as a function of temperature and depth with laws representative of upper and lower crust (Chapman, 1986). The thermal conductivity of sediments is a function of porosity and grain conductivity, which for siliciclastic sediment is strongly dependent on quartz content. A value of $2.5 \text{ W m}^{-1} \text{ K}^{-1}$ corresponding to $\sim 80\%$ clay and 20% sand is assumed, but this parameter may be consid-

¹GSA Data Repository item 2012006, Figure DR1 (exact geometries of basin models) and Table DR1 (values of thermal model parameters), is available online at www.geosociety.org/pubs/ft2012.htm, or on request from editing@geosociety.org or Documents Secretary, GSA, P.O. Box 9140, Boulder, CO 80301, USA.

ered adjustable between 2 and $3 \text{ W m}^{-1} \text{ K}^{-1}$. The initial conditions at the beginning of sedimentation correspond to a thermally equilibrated crust.

RESULTS

The steady-state model (Fig. 3B) is based on the extrapolation of the Holocene subsidence rate along the spring (2007) heat flow profile (NNE-SSW) over the past 2 Ma. The computed minimum heat flow at the depocenter fits the data for a basal heat flow of 53 mW/m^2 . However, the calculated heat flow is underestimated by $\sim 5 \text{ mW/m}^2$ in the north of the basin and overestimated by $5\text{--}10 \text{ mW/m}^2$ in the south of the basin. This may be explained by a variation of the subsidence pattern with time, or by a lateral variation of the initial basement heat flow that would be higher in the north than in the south of the basin. While this cannot be excluded, we consider it unlikely because the regional heat flow tends to increase southward. Furthermore, there is evidence that crustal extension has reduced crustal thickness from 35 km to 25 km (Bécel et al., 2009) south of the deep Sea of Marmara basins, and this should contribute to increased heat flow there.

Model II (Fig. 3A) is based on an interpretation of the seismic reflection profile, where sequences are identified. The top sequence S1 corresponds to a set of horizons with a shape in agreement with the constant subsidence rate model over the last 250 ka. Deeper horizons form a fan thickening northward toward F3, and two sequences with basal onlaps (S2 and S3) are recognized. The age of these sequences is estimated to be 450 and 640 ka applying the constant subsidence rate model to the shallow portion of the fan (Fig. 3A). The basal horizon of the Central Basin is defined following the deepest reflections attributable to syntectonic sedimentation, and within 1 km of the basement depth inferred from wide-angle study (Bécel et al., 2010). The age assigned to the basal horizon in the model defines the onset of subsidence. Results are shown for a crustal heat flow of 68 mW/m^2 and assumed ages of 5 Ma and 2 Ma for the basal horizon (Fig. 3B), and for a composite model assuming 5 Ma in the south and 2 Ma in the center and in the north of the basin. Compared with the steady-state subsidence model, a higher crustal heat flow is now required to fit the heat flow data. This is primarily due to the imposed acceleration of subsidence between 450 and 640 ka in the center of the basin. This taken into account, only the composite model fits data both on the north and on the south sides of the basin. We believe that the onset of subsidence cannot be accurately determined from thermal modeling due to ambiguity between model parameters (basal heat flow, thermal conductivity, and sedimentation rate). However, all models we tested that reproduce heat flow data and satisfy geometrical constraints from seismic studies indicate an earlier onset of subsidence (ranging from 5 to 3.5 Ma) in the south than in the center and the north of the basin (ranging from 2.5 to 1.5 Ma) and, at least at the location of the seismic profile, an episode of faster subsidence in the center of the Central Basin.

DISCUSSION AND CONCLUSION

The purpose of this discussion is to relate the finding of asymmetric and time-varying subsidence in the Central Basin with the current understanding of the tectonic framework. The fault network in the Sea of Marmara region may be geometrically subdivided into several subsystems. The Main Marmara fault (MMF) comprises the Ganos segment, the Çınarcık segment, and their connection, and presumably takes most of the present-day strike-slip motion (e.g., Le Pichon et al., 2003; Hergert and Heidbach, 2010). A discontinuous en echelon system, which we call the Central fault system (CFS) is observed in the prolongation of the Izmit fault (Carton et al., 2007) but has unclear westward termination and present-day kinematic importance. South of the CFS, tilted blocks bounded by low-angle normal faults (Bécel et al., 2010) extend in an area that we here call the South Transensional Zone (STZ, Fig. 1). The STZ contributed to early crustal stretching (Bécel et al., 2010) and probably also accommodated some transensional deformation. The eastern part of the STZ comprises active faults around Imrali Basin (Armijo et al., 2002), but its

western part shows little evidence for recent motion. A nearly continuous fault system with poorly constrained kinematics is also identified on the southern shelf (Parke et al., 2002). In this context, we propose that the southern subbasin of the Central Basin may have formed from extension within the STZ (in which case fault F5 is antithetic to the STZ northeast-dipping detachment) or at an extensional stepover between the Ganos segment (Fig. 1) and the CFS. A combination of both processes is also possible. The later onset of subsidence in the north is hypothetically related to a later development of strain in the MMF area. Subsidence in the center and in the north of the Central Basin is thus attributable to a releasing bend on the MMF and to slip on fault branches connected to the MMF, such as the northward bounding fault (Fig. 1). The change of subsidence pattern ca. 250 ka could possibly be related to a recent connection of the Ganos and North Çınarcık segments of the MMF (Rangin et al., 2004) or to fault interactions (Nicol et al., 2009).

Distribution of seafloor subsidence in the Sea of Marmara Central Basin apparently followed the same pattern over the last 250 ka, but varied continuously over a longer time scale. Furthermore, the Central Basin appears to be composed of two subbasins: a southern subbasin where subsidence initiated earlier (5–3.5 Ma) than in a northern subbasin (2.5–1.5 Ma). This evolution could be related to a northward migration of the zone of maximum lithospheric strain. Alternatively, it may represent a smaller-scale process associated with the initiation of the intrabasin faults F3 and F4. Comparable evolutions are observed in analog models of strike-slip basins with ductile decoupling in the crust (Smit et al., 2008).

ACKNOWLEDGMENTS

We thank Naci Görür, Celal Şengör, and Namik Çağatay for their constant support over the years of Turkish-French collaborative projects. We thank GENAVIR, IFREMER, INSU support teams, and the Turkish Navy for their help during the MARNAUT and MARMESONET cruises; and IFREMER, CNRS/INSU, and EC FP6 (ESONET) for funding. We thank Jean-Paul Callot, Jean-Marc Daniel, and Benoit Erout for their help, and supply of the TEMIS 2D 5.1.1 software. We thank Xavier Le Pichon, Claude Rangin, Alfred Hirn, and Mireille Laigle for stimulating discussions and comments, and J. Bull and M. Kinoshita for their reviews.

REFERENCES CITED

- Armijo, R., Meyer, B., Hubert, A., and Barka, A., 1999, Westward propagation of the North Anatolian fault into the northern Aegean: Timing and kinematics: *Geology*, v. 27, p. 267–270, doi:10.1130/0091-7613(1999)027<0267:WPOTNA>2.3.CO;2.
- Armijo, R., Meyer, B., Navarro, S., King, G., and Barka, A., 2002, Asymmetric slip partitioning in the Sea of Marmara pull-apart: A clue to propagation processes of the North Anatolian Fault?: *Terra Nova*, v. 14, p. 80–86, doi:10.1046/j.1365-3121.2002.00397.x.
- Bécel, A., Laigle, M., de Voogd, B., Hirn, A., Taymaz, T., Galve, A., Shimamura, H., Murai, Y., Lepine, J.C., Sapin, M., and Ozalaybey, S., 2009, Moho, crustal architecture and deep deformation under the North Marmara Trough, from the SEISMARMARA Leg 1 offshore-onshore reflection-refraction survey: *Tectonophysics*, v. 467, p. 1–21, doi:10.1016/j.tecto.2008.10.022.
- Bécel, A., Laigle, M., de Voogd, B., Hirn, A., Taymaz, T., Yolsal-Cevikbilen, S., and Shimamura, H., 2010, North Marmara Trough architecture of basin infill, basement and faults, from PSDM reflection and OBS refraction seismics: *Tectonophysics*, v. 490, p. 1–14, doi:10.1016/j.tecto.2010.04.004.
- Beck, C., and 14 others, 2007, Late Quaternary co-seismic sedimentation in the Sea of Marmara's deep basins: *Sedimentary Geology*, v. 199, p. 65–89, doi:10.1016/j.sedgeo.2005.12.031.
- Çağatay, M.N., Görür, N., Polonia, A., Demirbag, E., Sakıncı, M., Cormier, M.H., Capotondi, L., McHugh, C., Emre, Ö., and Eris, K., 2003, Sea-level changes and depositional environments in the Izmit Gulf, eastern Marmara Sea, during the late glacial–Holocene period: *Marine Geology*, v. 202, p. 159–173, doi:10.1016/S0025-3227(03)00259-7.
- Çağatay, M.N., Eris, K., Ryan, W.B.F., Sancar, Ü., Polonia, A., Akçer, S., Biletkin, D., Gasperini, L., Görür, N., Lericolais, G., and Bard, E., 2009, Late Pleistocene–Holocene evolution of the northern shelf of the Sea of Marmara: *Marine Geology*, v. 265, p. 87–100, doi:10.1016/j.margeo.2009.06.011.
- Carton, H., Singh, S.C., Hirn, A., Bazin, S., de Voogd, B., Vigner, A., Ricolleau, A., Cetin, S., Oçakoglu, N., Karakoc, F., and Sevilgen, V., 2007, Seismic imaging of the three-dimensional architecture of the Çınarcık Basin along the North Anatolian Fault: *Journal of Geophysical Research, Solid Earth*, v. 112, B06101, doi:10.1029/2006JB004548.
- Chapman, D.S., 1986, Thermal gradients in the continental crust: *The Geological Society of London Special Publication* 24, p. 63–70.
- Hergert, T., and Heidbach, O., 2010, Slip-rate variability and distributed deformation in the Marmara Sea fault system: *Nature Geoscience*, v. 3, p. 132–135, doi:10.1038/ngeo739.
- Hubert-Ferrari, A., King, G., Manighetti, I., Armijo, R., Meyer, B., and Tapponnier, P., 2003, Long-term elasticity in the continental lithosphere; modelling the Aden Ridge propagation and the Anatolian extrusion process: *Geophysical Journal International*, v. 153, p. 111–132, doi:10.1046/j.1365-246X.2003.01872.x.
- Hutchison, I., 1985, The effects of sedimentation and compaction on oceanic heat flow: *Geophysical Journal of the Royal Astronomical Society*, v. 82, p. 439–459.
- Hutchinson, M.F., and Dowling, T.I., 1991, A continental hydrological assessment of a new grid-based digital elevation model of Australia: *Hydrological Processes*, v. 5, p. 45–58, doi:10.1002/hyp.3360050105.
- Laigle, M., Bécel, A., de Voogd, B., Hirn, A., Taymaz, T., Ozalaybey, S., and Team, S.L., 2008, A first deep seismic survey in the Sea of Marmara: Deep basins and whole crust architecture and evolution: *Earth and Planetary Science Letters*, v. 270, p. 168–179, doi:10.1016/j.epsl.2008.02.031.
- Le Pichon, X., Henry, P., and Lallemand, S., 1990, Water flow in the Barbados accretionary complex: *Journal of Geophysical Research, Solid Earth and Planets*, v. 95, p. 8945–8967, doi:10.1029/JB095iB06p08945.
- Le Pichon, X., Şengör, A.M.C., Demirbag, E., Rangin, C., Imren, C., Armijo, R., Görür, N., Çağatay, N., de Lepinay, B.M., Meyer, B., Saatçılar, R., and Tok, B., 2001, The active Main Marmara Fault: *Earth and Planetary Science Letters*, v. 192, p. 595–616, doi:10.1016/S0012-821X(01)00449-6.
- Le Pichon, X., Chamot-Rooke, N., Rangin, C., and Şengör, A.M.C., 2003, The North Anatolian fault in the Sea of Marmara: *Journal of Geophysical Research, Solid Earth*, v. 108, 2179, doi:10.1029/2002JB001862.
- Lisiecki, L.E., and Raymo, M.E., 2005, A Pliocene–Pleistocene stack of 57 globally distributed benthic $\delta^{18}\text{O}$ records: *Paleoceanography*, v. 20, PA1003, doi:10.1029/2004PA001071.
- Lucaszeu, F., and Le Douaran, S., 1985, The blanketing effect of sediments in basins formed by extension: A numerical model. Application to the Gulf of Lion and Viking graben: *Earth and Planetary Science Letters*, v. 74, p. 92–102, doi:10.1016/0012-821X(85)90169-4.
- Muller, J.R., and Aydin, A., 2005, Using mechanical modeling to constrain fault geometries proposed for the northern Marmara Sea: *Journal of Geophysical Research, Solid Earth*, v. 110, B03407, doi:10.1029/2004JB003226.
- Nicol, A., Walsh, J., Mouslopoulou, V., and Villamor, P., 2009, Earthquake histories and Holocene acceleration of fault displacement rates: *Geology*, v. 37, p. 911–914, doi:10.1130/G25765A.1.
- Parke, J.R., Minshull, T.A., Anderson, G., White, R.S., McKenzie, D., Kucsu, I., Bull, J.M., Görür, N., and Şengör, C., 1999, Active faults in the Sea of Marmara, western Turkey, imaged by seismic reflection profiles: *Terra Nova*, v. 11, p. 223–227, doi:10.1046/j.1365-3121.1999.00248.x.
- Parke, J.R., White, R.S., McKenzie, D., Minshull, T.A., Bull, J.M., Kucsu, I., Görür, N., and Şengör, C., 2002, Interaction between faulting and sedimentation in the Sea of Marmara, western Turkey: *Journal of Geophysical Research, Solid Earth*, v. 107, 2286, doi:10.1029/2001JB000450.
- Pfister, M., Rybach, L., and Simsek, S., 1998, Geothermal reconnaissance of the Marmara Sea region (NW Turkey): Surface heat flow density in an area of active continental extension: *Tectonophysics*, v. 291, p. 77–89, doi:10.1016/S0040-1951(98)00032-8.
- Rangin, C., Le Pichon, X., Demirbag, E., and Imren, C., 2004, Strain localization in the Sea of Marmara: Propagation of the North Anatolian Fault in a now inactive pull-apart: *Tectonics*, v. 23, TC2014, doi:10.1029/2002TC001437.
- Rudkiewicz, J.-L., Penteado, H.L.B., Vear, A., Vandenbroucke, M., Brigaud, F., Wendebourg, J., and Düppenbecker, S., 2000, Integrated basin modeling helps to decipher petroleum systems: *American Association of Petroleum Geologists Memoir* 73, p. 27–40.
- Seeber, L., Cormier, M.H., McHugh, C., Emre, O., Polonia, A., and Sorlien, C., 2006, Rapid subsidence and sedimentation from oblique slip near a bend on the North Anatolian transform fault in the Marmara Sea, Turkey: *Geology*, v. 34, p. 933–936, doi:10.1130/G22520A.1.
- Şengör, A.M.C., 1985, The story of Tethys: How many wives did Okeanos have?: *Episodes*, v. 8, p. 3–12.
- Şengör, A.M.C., Tuysuz, O., Imren, C., Sakıncı, M., Eyidoğan, H., Görür, G., Le Pichon, X., and Rangin, C., 2005, The North Anatolian Fault: A new look: *Annual Review of Earth and Planetary Sciences*, v. 33, p. 37–112, doi:10.1146/annurev.earth.32.101802.120415.
- Siddall, M., Rohling, E.J., Almogi-Labin, A., Hemleben, C., Meischner, D., Schmelzer, I., and Smeed, D.A., 2003, Sea-level fluctuations during the last glacial cycle: *Nature*, v. 423, p. 853–858, doi:10.1038/nature01690.
- Smit, J., Brun, J.P., Cloetingh, S., and Ben-Avraham, Z., 2008, Pull-apart basin formation and development in narrow transform zones with application to the Dead Sea Basin: *Tectonics*, v. 27, TC6018, doi:10.1029/2007TC002119.

Manuscript received 21 February 2011

Revised manuscript received 2 August 2011

Manuscript accepted 3 August 2011

Printed in USA